Journal of Power Sources 267 (2014) 58–68

Contents lists available at ScienceDirect

Journal of Power Sources

journal homepage: www.elsevier.com/locate/jpowsour

Quantitative analysis of solid oxide fuel cell anode microstructure change during redox cycles

Takaaki Shimura [a, *], Zhenjun Jiao [a, b], Shotaro Hara [a, b], Naoki Shikazono [a, b, 1]

[a] Institute of Industrial Science, The University of Tokyo, Komaba 4-6-1, Meguro-ku, Tokyo 153-8505, Japan
[b] CREST, JST Gobancho 7, Chiyoda-ku, Tokyo 102-0076, Japan

HIGHLIGHTS

- Performance was enhanced and TPB density increased after redox treatment.
- Performance degraded and TPB density decreased after discharge process.
- As redox cycles are repeated, gradual degradation was observed.
- TPB density increased as the redox cycles are repeated.
- Performance degradation cannot be explained from microstructure change.

ARTICLE INFO

Article history:
Received 6 March 2014
Received in revised form
19 April 2014
Accepted 30 April 2014
Available online 21 May 2014

Keywords:
Solid oxide fuel cell
Ni-YSZ
Redox
Microstructure
FIB-SEM

ABSTRACT

In the present study, correlation between solid oxide fuel cell anode microstructure and electrochemical performance during redox cycles was investigated. Electrolyte-support cell with nickel/yttria stabilized zirconia composite anode was prepared and tested under discharge process with redox cycles. Redox treatment was basically conducted every 20 h during discharge process. Polarization resistance decreased just after redox treatment and increased during discharge process. Enhancement of cell performance after every redox cycles and faster degradation in the following discharge process were observed. Polarization resistance gradually increased as redox cycles were repeated. Focused ion beam-scanning electron microscopy (FIB-SEM) observation was conducted for reconstructing the three dimensional microstructures of the tested samples. From the three dimensional microstructure reconstruction, it is found that the shape of nickel particle got thinner and complicated after redox cycles. Triple phase boundary (TPB) length increased after redox treatment and decreased after discharge process. This TPB change was highly associated with Ni connectivity and Ni specific surface area. These microstructure changes are consistent with the change of cell performance enhancement after redox treatment and degradation after discharge process. However, TPB length density kept on increasing as redox cycles are repeated, which is inconsistent with the gradual degradation of anode performance.

1. Introduction

Nickel/yttria stabilized zirconia (Ni-YSZ) cermet is the most common material for the solid oxide fuel cell (SOFC) anode. To ensure high performance of SOFC for a long operation time, cell and system designs which have sufficient durability against cyclic reduction and oxidation (redox) of anode are essential. Redox is caused when chemical potential of oxygen increases in the anode side in cases such as high fuel utilization, gas leakage from the cathode side and fuel interruption [1–9]. The decrease of volume during reduction from NiO to Ni is as about 40%, and the increase of volume is about 70% during oxidation [3–5]. This Ni volume change leads to irreversible microstructure change and bulk deformation of Ni-YSZ anode and causes cracks inside the electrolyte in the most severe situation [1–9]. Sumi et al. [10] reported increase of polarization impedance after redox cycles with the decrease of TPB length and increase of Ni specific surface area. Increase of polarization resistance was also reported by Laurencin et al. [8]. Jeangros et al. [11] carried out in-situ observation during redox states of Ni-YSZ sample using ETEM and confirmed how Ni particle became

* Corresponding author. Tel./fax: +81 354526777.
E-mail addresses: tshimura@iis.u-tokyo.ac.jp (T. Shimura), shika@iis.u-tokyo.ac.jp (N. Shikazono).
[1] Tel./fax: +81 354526776.

http://dx.doi.org/10.1016/j.jpowsour.2014.04.152
0378-7753/

porous and dense through re-oxidation and re-reduction processes. From the in-situ observation, they proposed a schematic mechanism of redox microstructure change, i.e. Ni diffusion becomes dominant during oxidation process which creates inner pore, whereas surface reaction is dominant during reduction process accompanying spongy-like Ni structure [7]. Regarding chemical reaction mechanism, Tikekar et al. [12] investigated on rate-determining kinetics of Ni oxidation and NiO reduction in various conditions. Rate determining process during redox atmosphere is also examined and high dependency on temperature and gas composition is reported [13,14]. Redox durability is strongly related with initial microstructure of anode. To prevent microstructure change during redox cycles, composite anodes with various dopants are examined [15]. In addition, redox dependency on temperature is also investigated by the same authors [16]. Nevertheless, precise mechanism of redox cycle has not been fully understood due to its high dependency on cell design, experimental conditions, etc.

Understanding the details of relationship between microstructure change and cell performance during redox cycles is necessary to reveal redox kinetics. In this work, discharge tests were conducted with and without redox treatment to clearly identify the effects of redox cycles. The three-dimensional microstructures of the samples were analyzed using FIB-SEM observation technique.

2. Experimental procedure

2.1. Electrolyte support cell fabrication

8YSZ disc (Tosoh Japan) of 24 mm in diameter was used as an electrolyte. Slurries for Ni-8YSZ composite anode, Ni anode current collecting layer, LSM-8YSZ composite cathode, LSM cathode current collecting layer (AGC Seimi Chemical, Japan), were each mixed with terpineol solvent and 3 wt% ethylcellulose binder. Then, they were screen printed onto the YSZ disc to form ϕ 10 mm electrode. Electrodes were sintered in the electric oven in air atmosphere. Sintering temperature was 1450 °C for the anode and 1200 °C for the cathode.

2.2. SOFC operation test

Fabricated cell was set inside the test rig. Pt reference electrode was fixed around the side of the electrolyte disk. Temperature was kept at 800 °C during cell operation test. Initially, anode was reduced with nitrogen diluted hydrogen. Then 5% humidified hydrogen and pure oxygen were supplied to anode and cathode sides, respectively. Current–Voltage and impedance measurements were conducted using Solatron 1287 and Solatron 1255B. Impedance measurement was conducted for every 20 h. Between the impedance measurements, cell was discharged under constant current of 0.2 A cm^{-2}. For the tests with-redox cycles, impedance measurements were also conducted before and after each redox treatment.

Pure oxygen is introduced for 2 h during the oxidation process, and pure hydrogen is introduced for 1 h during the reduction process. Nitrogen was flushed when switching gas supply from oxygen to hydrogen. Electrochemical measurements were conducted before and after 20 h discharge process. Oxidation time was set to achieve full Ni oxidation, and we confirmed that Ni is fully oxidized after 2 h oxidation from the EDX analysis. Operation was conducted with several different sequences to evaluate the influences of redox cycles. Cell operation conditions are shown in Table 1. First test consists of 5 sets of 20 h discharge without redox treatment (100 h discharge test, hereafter), as a reference case. Second one was carried out with 5 sets of 20 h discharge processes with 4 redox treatments held every 20 h between the discharge processes (4 redox test). Third test was conducted to confirm degradation ratio after single redox treatment, in which continuous 80 h discharge was conducted after initial 20 h discharge and following single redox treatment (1 redox test). Total discharge time is 100 h for these three tests.

Table 1
Cell operation condition.

Test name	Operation sequence
100 h discharge test	5 × 20 h discharge
4 redox test	20 h discharge + 4× (redox + 20 h discharge)
1 redox test	20 h discharge + redox + 4 × 20 h discharge
10 redox test	20 h discharge + 10× (redox + 20 h discharge[a])

[a] Discharge time for 2nd and 5th redox cycles are 19 h.

In addition, to confirm the accumulated redox treatment influence on cell performance, longer operation was conducted with 10 redox cycles (10 redox test). Basic experimental condition is the same with the "4 redox test", except that oxidation was 3 h for the initial redox, and the discharge time after 2nd and 5th redox cycles were 19 h

2.3. Microstructure analysis

After the experiment, each anode sample was filled with epoxy resin (Struers Epofix), and polished with sand paper and cross section polisher (JEOL SM-09020CP). Then, series of cross sectional images were taken by FIB-SEM (NVision 40, SII Nanotechnology) [17]. Each image data was converted to ternarized images and merged to 3D voxel structures to calculate microstructural parameters. Calculated parameters are porosity, connectivity from the electrolyte to the current collector, total and active TPB densities, interception lengths, specific surface area and tortuosity factor. Calculation methods of each parameter are described in Refs. [17–21].

3. Results and discussion

3.1. Electrochemical performance change

Temporal changes of anode-reference voltage are shown in Fig. 1. Interruptions of each line correspond to the periods of

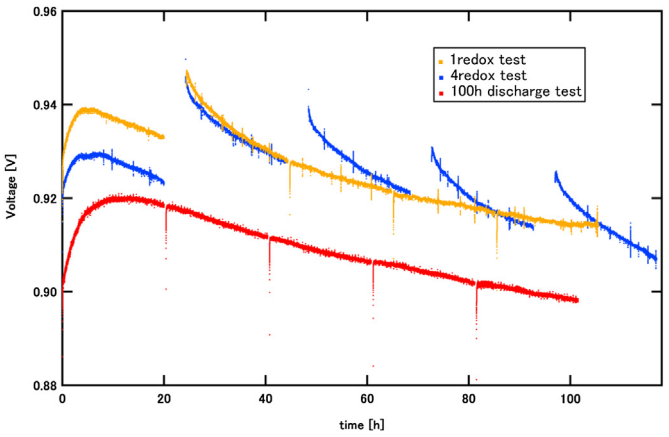

Fig. 1. Anode-reference voltage change during Redox tests. "100 h discharge test" (red), "4 redox test" (blue) and "1 redox test" (orange). (For interpretation of the references to color in this figure legend, the reader is referred to the web version of this article).

electrochemical impedance measurements and redox treatments. The difference of initial voltages are due to the variation between the cells. In every test, voltage increased during the early stage of the discharge process. This is probably due to the anode microstructure change which took place at the very initial stage of operation. For the "100 h discharge test" (red line), gradual voltage decrease is observed. On the other hand, for the "4 redox test" (blue line), performance enhancement after each redox treatment, and faster degradation at subsequent discharge process were observed. Furthermore, for the "1 redox test" (orange line), fast initial degradation after redox treatment converges to the same level of the "100 h discharge test". These results imply that single redox treatment affects degradation rate temporally, but has little influence on long discharge operation. This behavior is different from the past work which reports voltage drop just after every redox cycle [22]. Regarding the enhancement just the after redox treatment, Pihlatie et al. [16] measured electronic conductivity of Ni-YSZ cermet and observed an increase of conductivity after the redox

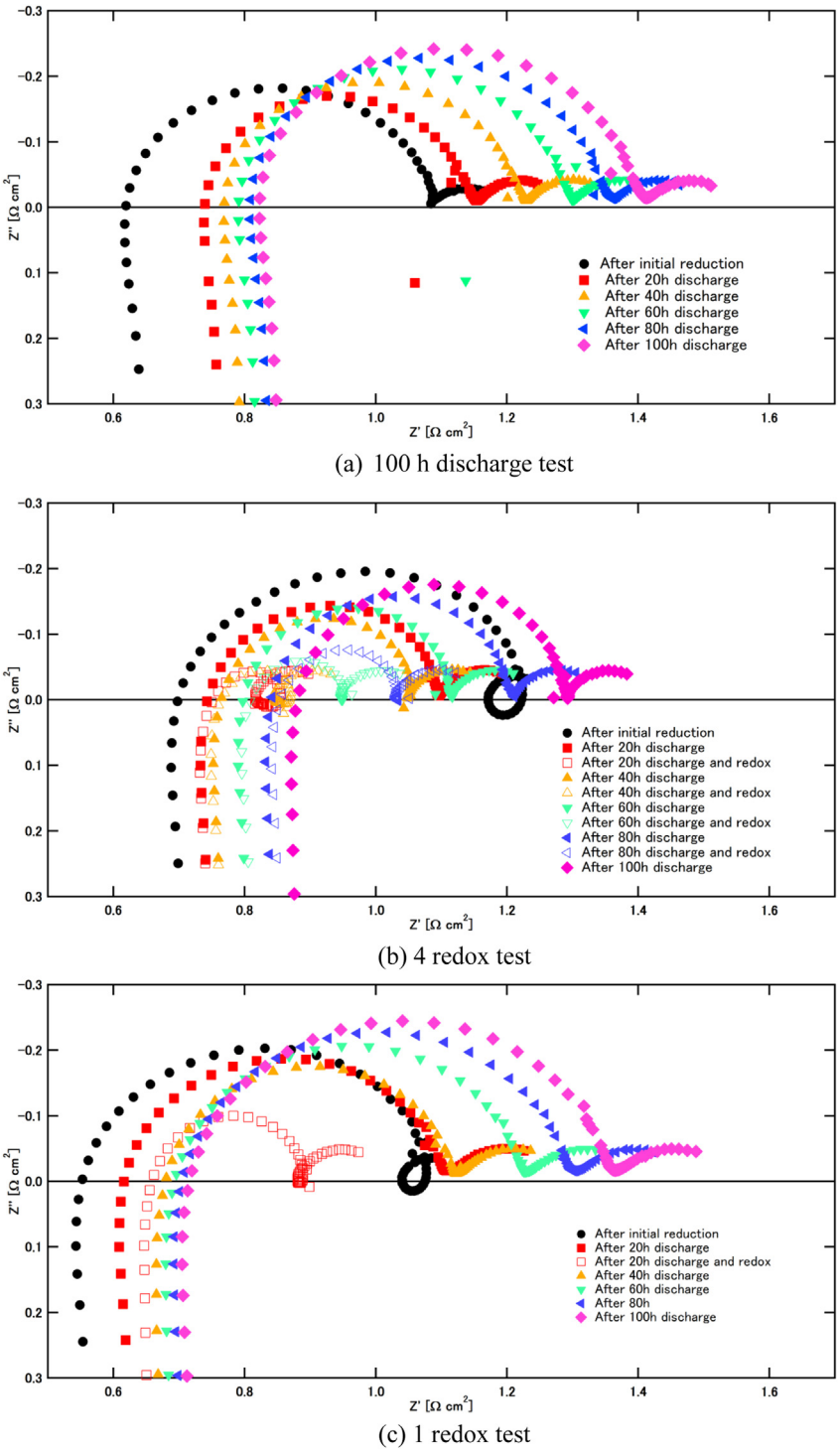

Fig. 2. Anode-reference impedance measurement during cell operation test.

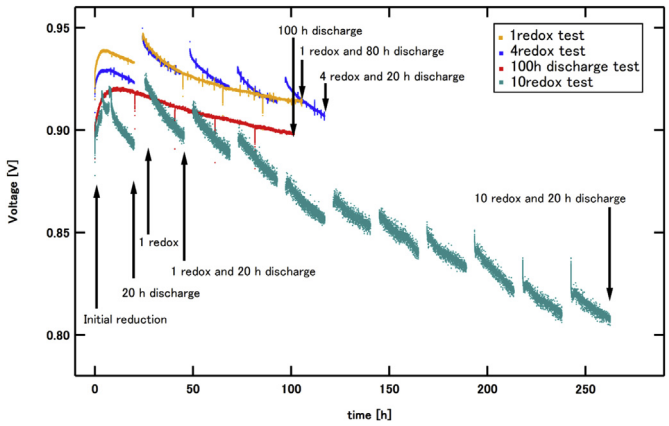

Fig. 3. Anode-reference voltage change during 10 redox test. Other tests are also shown for reference.

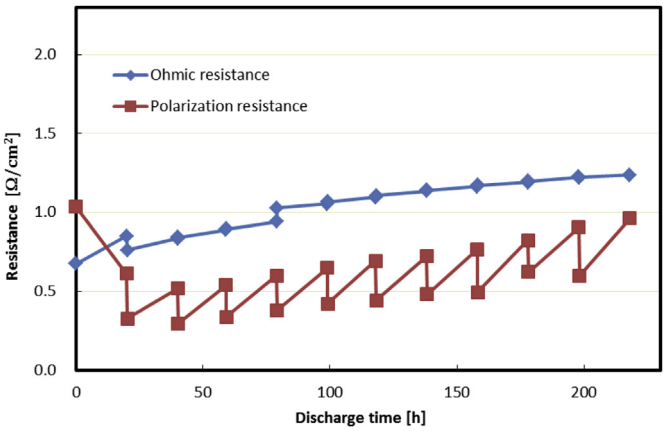

Fig. 5. Changes of ohmic and polarization resistances during 10 redox test.

treatment. This phenomena can be explained by the increase of Ni connectivity. Of course, this discussion is not simply applied to the electrode total performance, in which not only electron transportation, but also ionic transportation and gas diffusion are associated.

Polarization and ohmic resistances both gradually increased during "100 h discharge test", as shown in Fig. 2 (a). On the other hand, from the impedance results of "4 redox test", decrease of polarization resistance just after redox treatment and increase of polarization resistance after subsequent discharge process are clearly observed, as shown in Fig. 2(b). These are also consistent with the voltage change shown in Fig. 1. Change of polarization resistance is found mostly on high frequency region which is considered to be related to the charge transfer reaction. From the result of "1 redox test" in Fig. 2(c), polarization resistance decreased after 1st redox, then it kept increasing throughout the following discharge process. Thus, enhancement of performance and following rapid degradation are also clearly observed from the impedance measurement. Decrease of polarization resistance just after redox treatment is also reported at lower temperature [23]. Ohmic resistance increased for all tests, but they are not distinctively different from the "100 h discharge test" result.

Voltage change during the "10 redox cycle test" was similar to that of the "4 redox test", as shown in Fig. 3. Increase of voltage after redox treatment and decrease during subsequent discharge process were observed for the whole operation.

Impedance data was analyzed by equivalent-circuit fitting using ZPlot. Equivalent circuit consists of inductance (L1) resistance (R1), two RQ elements and Warburg impedance (Ws1) as shown in Fig. 4. Polarization resistance is defined as the total sum of R2, R3 and Ws1.

Result of impedance analysis is shown in Fig. 5. Ohmic resistance increased constantly through the whole discharge process. Little change was observed before and after redox treatment. Polarization resistance decreased just after redox and increased through the subsequent discharge process. Polarization resistance continuously increased through 10 redox cycles.

3.2. Microstructure analysis

To reveal the relationship between the electrode performance and the microstructure change, FIB-SEM observation was conducted. Eight different samples were prepared from cell pieces after different steps of operation. Those are, 1) after initial reduction, 2) after 20 h discharge, 3) after 1st redox, 4) after 1 redox and 20 h discharge, 5) after 100 h discharge without redox, 6) after 1 redox and 80 h discharge, 7) after 4 redox and 20 h discharge, and 8) after 10 redox and 20 h discharge. Observation points are indicated in Fig. 3 with arrows.

SEM images are shown in Fig. 6. From the SEM images of "initial reduction", "20 h discharge" and "100 h discharge" samples, we can see that Ni particles become round and large. This is consistent with the Ni microstructure change reported in Refs. [22,24,25]. From "1 redox" image, Ni particle changed to thinner and more elongated shape. This is a characteristic deformation caused after redox treatment, which is also reported in Ref. [10]. From "1 redox and 20 h discharge" and "1 redox and 80 h discharge" images, we can find that Ni particle get round and smooth again through the discharge process. From "4 redox cycles and 20 h discharge" and "10 redox and 20 h discharge" images, we can see that Ni particle shape got more and more complicated and fine. These microstructure change implies that drastic deformation of Ni is caused as a result of redox treatment, and gradual smoothing occurs through the discharge process. On the other hand, microstructure change of YSZ is visually unclear from these images.

Then, every image was ternarized using brightness values of Ni, YSZ, and pore phases. Ternarized images are stacked and converted to three dimensional voxel structures as shown in Fig. 7. Calculated microstructure parameters are shown in Table 2. In order to figure out microstructure change more clearly, some parameters are individually plotted against time and number of redox cycles.

In Fig. 8(a), porosity increased during the discharge process, except for the "100 h discharge test". This is probably due to the variations between the cells or FIB-SEM observation regions.

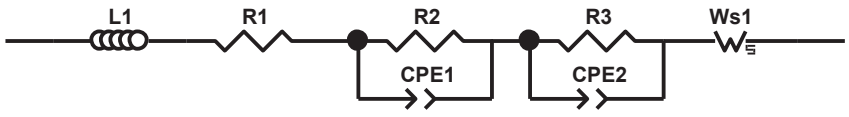

Fig. 4. Equivalent circuit model for impedance fitting. Consists of inductance (L1) resistance (R1), two RQ elements and Warburg impedance.

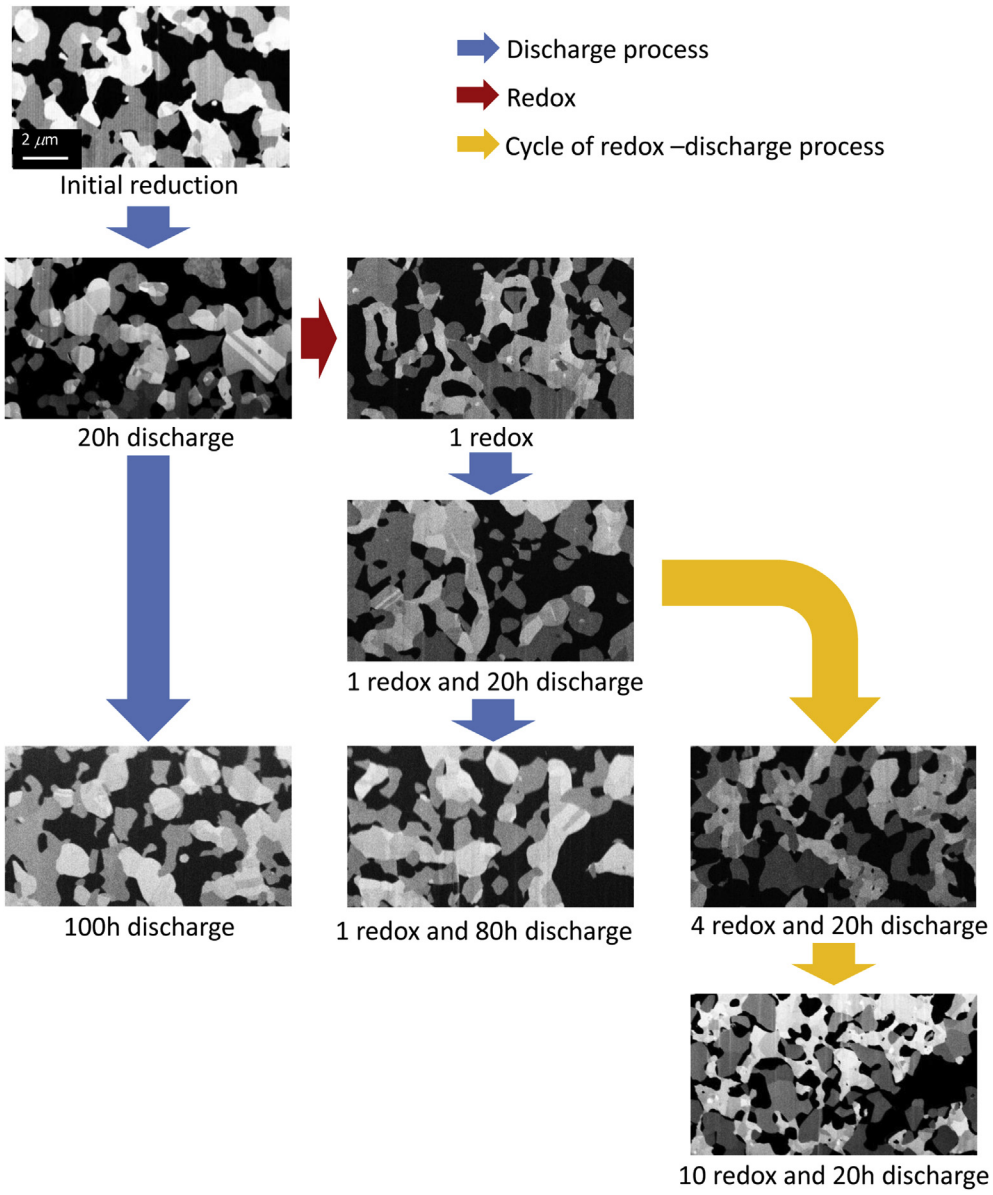

Fig. 6. SEM images of anode during redox testing. Ni appears as light gray, YSZ as dark gray and pore as black.

Increase of porosity during discharge process is also reported previously [25]. On the other hand, porosity decreased after redox treatments. For the "4 redox and 20 h discharge" sample, porosity was smaller than that of "100 h discharge" and "1 redox and 80 h discharge" samples. This result suggests that decrease of porosity during redox treatment is greater than the increase of porosity during the discharge process. As redox cycles are repeated, porosity kept on decreasing as shown in Fig. 8(b). This is contrary to the previously-reported result by Holzer et al. [26].

Temporal change of active TPB density is shown in Fig. 9 (a). Active TPB density decreased after the initial 20 h discharge process, and increased after the first redox treatment. Then, it decreased again during subsequent discharge process. For the "4 redox and 20 h discharge" sample, active TPB density shows higher value than that of "100 h discharge" sample. On the other hand, active TPB density of "1 redox and 80 h discharge" sample shows close value with that of "100 h discharge" sample. This result implies that impact of single redox treatment is small in the whole process.

Active TPB density increased as redox cycles are repeated as can be seen from Fig. 9(b). Active TPB density of "10 redox and 20 h discharge" sample was the largest among all the samples examined. On the other hand, as shown in Fig. 5, polarization resistance increased gradually during redox cycles. Thus, increase of active TPB density after redox cycles conflicts with the degradation of anode performance.

Changes of tortuosity factors are shown in Fig. 10. From Fig. 10(a), Ni tortuosity factor showed large decrease after the redox treatment and increase during the 20 h discharge process, although it decreased for the latter period of "100 h discharge" operation. Also, YSZ tortuosity factor showed a decrease after the redox treatment and an increase during the discharge process. As redox cycles are repeated, Ni tortuosity factor decreased as shown in Fig. 10(d). YSZ tortuosity factor showed a variation without showing any typical tendency by redox cycles. For the pore phase tortuosity, little change was observed in Fig. 10(c), but it became very large after "10 redox and 20 h discharge" as shown in Fig. 10(d).

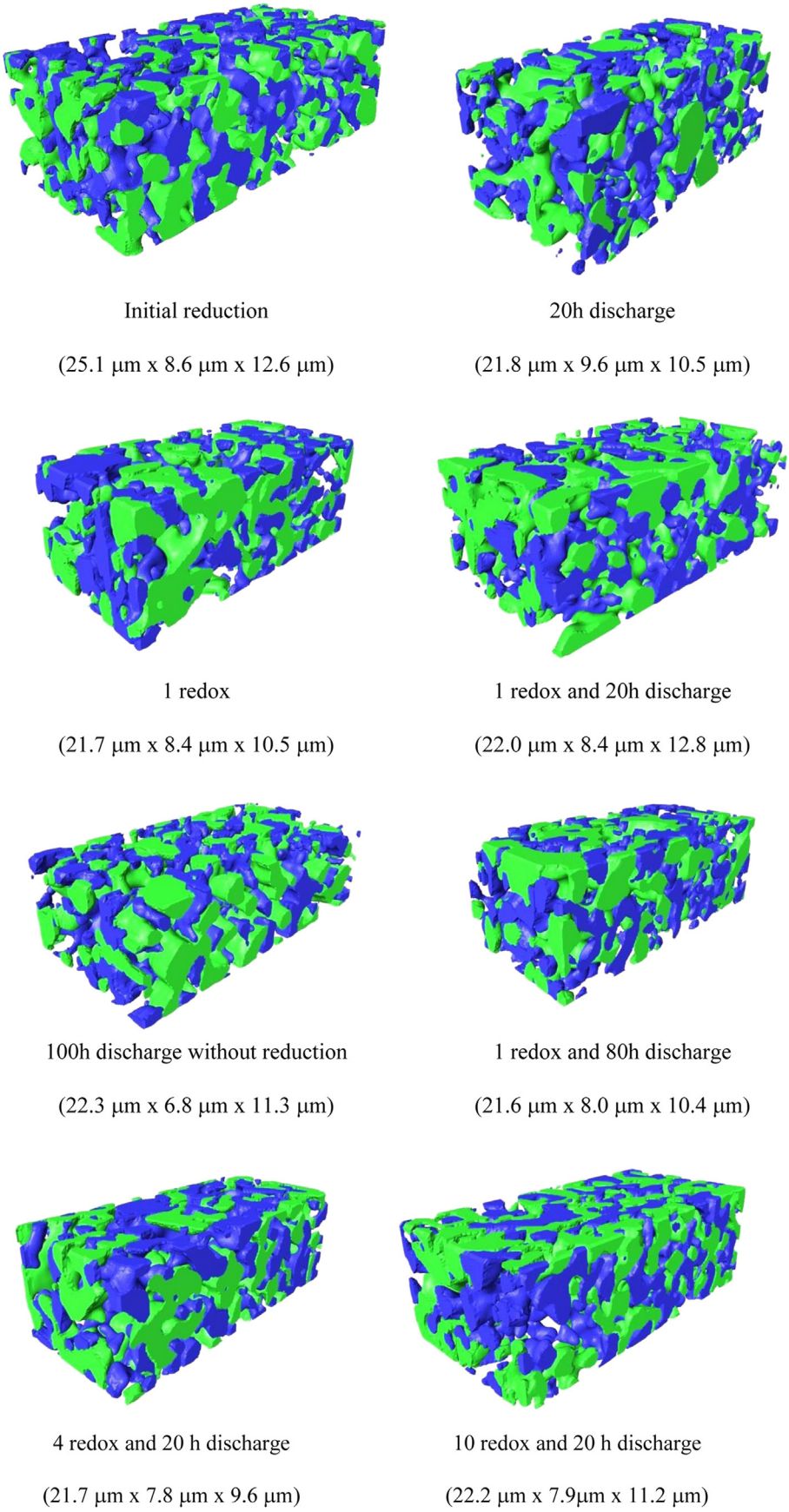

Fig. 7. Reconstructed 3D microstructures from FIB-SEM measurements. Green: Ni, Blue: YSZ. (For interpretation of the references to color in this figure legend, the reader is referred to the web version of this article).

Table 2
Calculated microstructure parameters.

		Initial reduction	20 h discharge	1 redox	1 redox and 20 h discharge	1 redox and 80 h discharge	4 redox and 20 h discharge	100 h Discharge	10 redox and 20 h discharge
Volume fraction (%)	Ni	26.27	25.72	25.55	25.97	26.47	27.21	26.82	33.79
	YSZ	28.01	25.86	29.86	28.49	26.36	30.40	25.61	30.31
	Pore	45.72	48.42	44.59	45.54	47.17	42.39	47.57	35.90
Connectivity (%)	Ni	96.09	92.92	98.14	95.78	94.39	99.33	89.82	99.65
	YSZ	97.34	96.39	96.75	97.14	96.76	96.22	96.25	93.46
	Pore	99.86	99.93	99.10	99.80	99.92	99.30	99.96	99.24
TPB density ($\mu m\ \mu m^{-3}$)	Total	2.47	2.51	2.46	2.15	2.19	2.61	2.53	3.79
	Active	1.89	1.65	1.93	1.64	1.58	2.08	1.64	2.83
Specific surface area ($\mu m^2\ \mu m^{-3}$)	Ni	1.31	1.19	1.38	1.15	1.15	1.45	1.21	2.07
	YSZ	2.00	2.03	1.80	1.89	1.97	1.96	2.09	1.99
Mean interception length (μm)	Ni	0.89	0.94	0.82	0.96	1.06	0.85	0.97	0.71
	YSZ	0.62	0.56	0.73	0.67	0.64	0.71	0.55	0.66
	Pore	0.96	0.99	0.93	0.96	1.09	0.82	0.97	0.57
Tortuosity factor	Ni	7.96	17.74	6.53	8.99	10.24	4.90	11.60	3.17
	YSZ	10.21	10.86	7.42	8.33	9.45	7.04	11.39	9.75
	Pore	2.43	2.10	2.75	2.61	2.57	3.22	2.18	7.24

4. Discussion

Densification of anode after redox cycles is considered to be highly related to the increase of pore tortuosity factor. By comparing "1 redox and 20 h discharge", "4 redox and 20 h discharge", and "10 redox and 20 h discharge" from Table 2, we can see that pore connectivity slightly decreased as redox cycles are repeated. Through this process, isolated pore might be formed. Furthermore, mean interception length of pore decreased as redox cycles. This also contributes to increase pore tortuosity factor.

Change of active TPB is considered to be highly associated with the change of Ni connectivity and Ni particle shape. From Fig. 11 (a) and (b), changes of Ni connectivity and Ni specific surface area show a trend similar to that of the active TPB density, i.e. both parameters show increase after redox treatment and decrease during discharge process. After redox treatment, Ni particle changed into thin and elongated shape as mentioned earlier. Elongated Ni particles are also reported in Ref. [10]. This microstructure change is also confirmed from the decrease of mean interception length and increase of specific surface area after redox

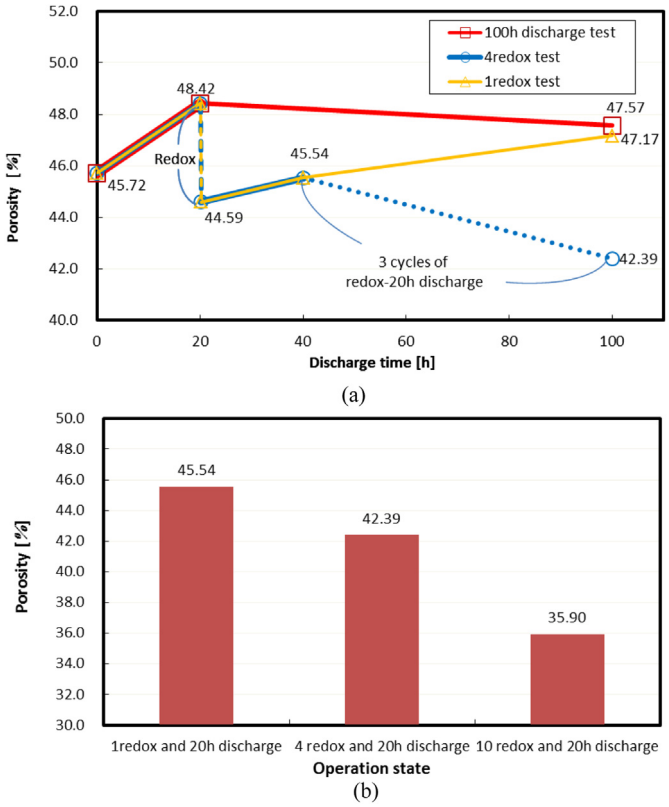

Fig. 8. Porosity change during cell operation. (a) Temporal change and (b) comparison for different number of redox cycles.

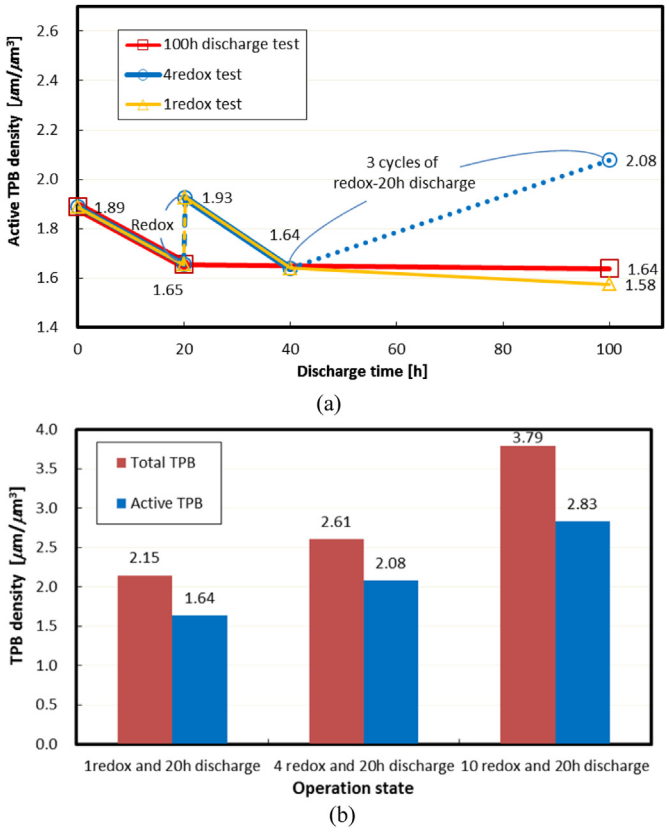

Fig. 9. TPB density change during cell operation. (a) Temporal change and (b) comparison for different number of redox cycles.

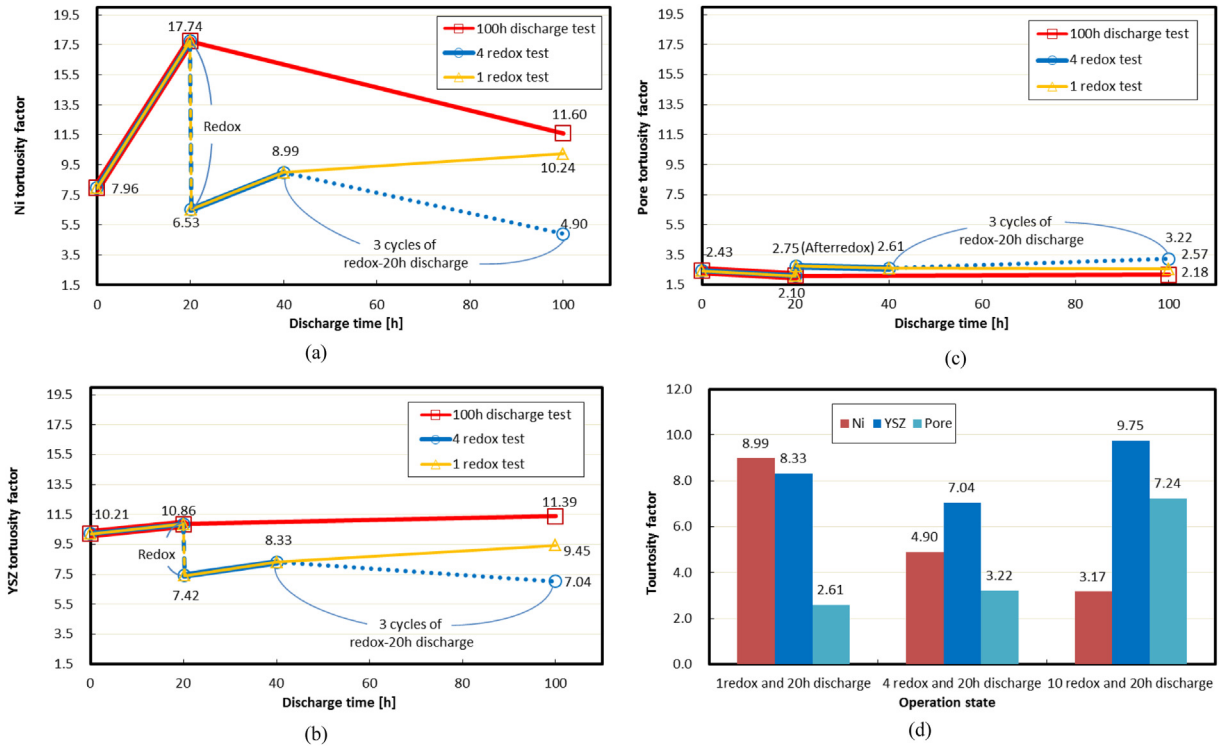

Fig. 10. Tortuosity factor changes during cell operation. Temporal changes of (a) Ni, (b) YSZ, and (c) pore, and (d) comparison for different number of redox cycles.

treatment from Fig. 11(b) and (c). It is also clearly shown in Fig. 12 (a) that Ni particle size gets smaller due to redox treatment. Elongated Ni particle enhances connection of Ni network, which contributes to the increase of active TPB density. Pihlatie et al. also reported an improvement of Ni network and an increase of conductivity after redox treatment [15,16]. Enhancement of conductivity was also reported by Klemenso et al. [1]. Furthermore, Ni particle volume fraction increases after redox treatment due to

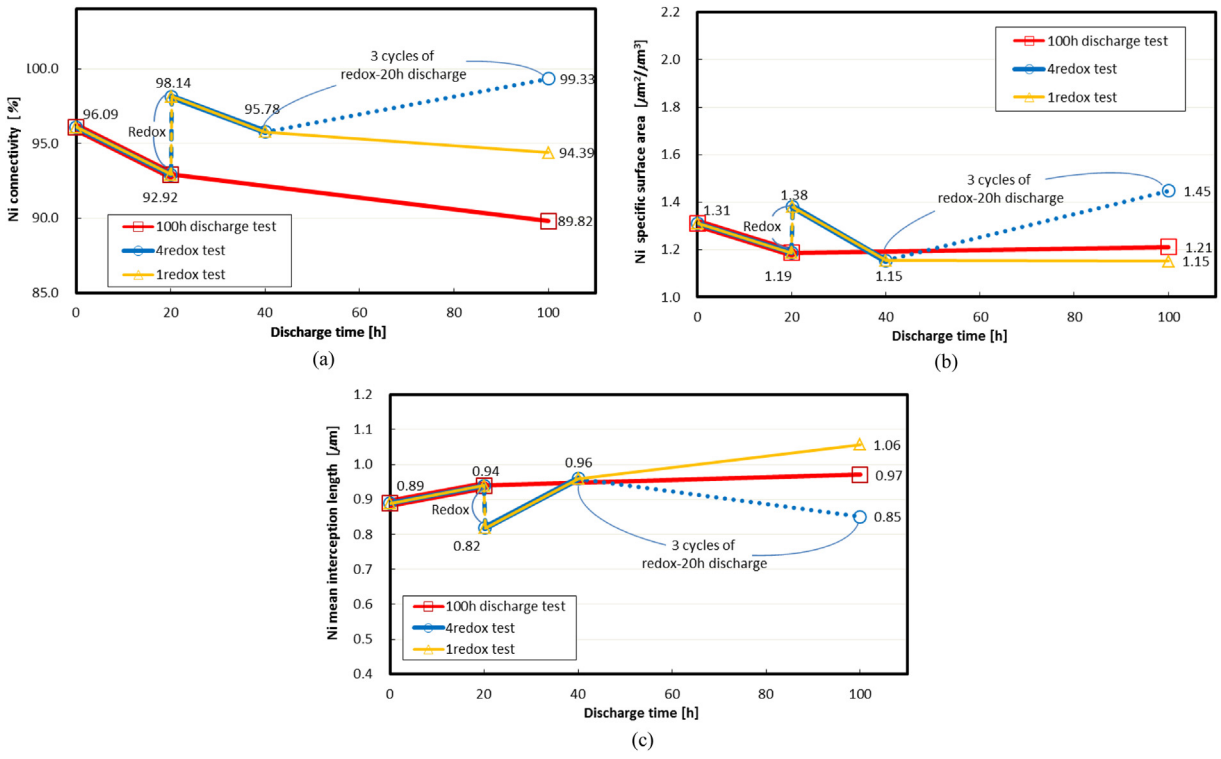

Fig. 11. Change of (a) Ni connectivity, (b) Ni specific surface area, and (c) Ni s mean interception length .

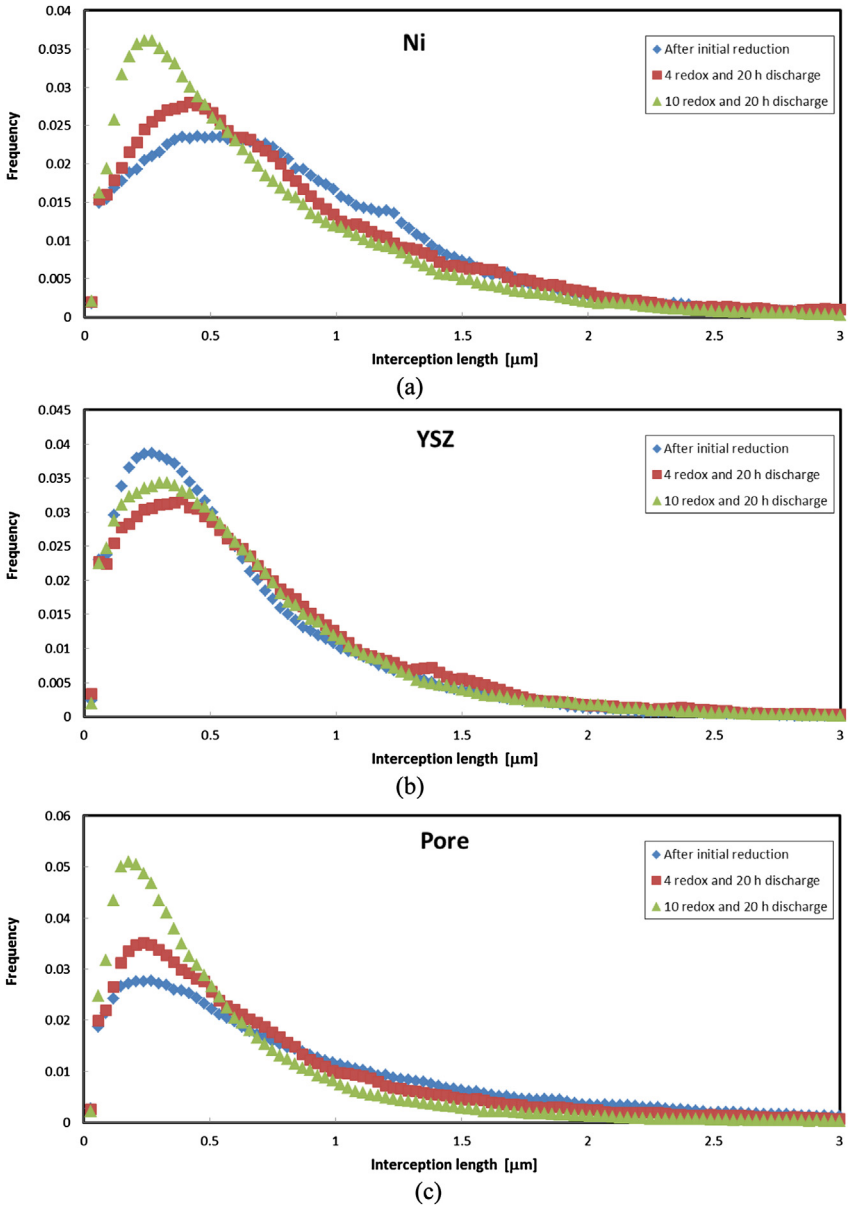

Fig. 12. Comparison of particle size distribution based on interception length for initial reduction, 4 redox and 20 h discharge, and 10 redox and 20 h discharge. (a) Ni, (b) YSZ, and (c) Pore.

densification of anode, which also contributes to improve Ni connectivity. During discharge process, sintering of Ni particle proceeds and particle grow into round and larger shape. Mean interception length also increases and specific surface area decreases during the discharge process. As sintering of Ni promotes isolation of Ni particle, active TPB density decreases. This is consistent with the result of impedance analysis, i.e. polarization resistance increased during discharge process and decreased after redox treatment. As redox cycles are repeated, Ni connectivity and Ni specific surface area increases, and mean interception length of Ni decreases, which contributes to the increase of active TPB.

Generally, redox is a major cause of YSZ structure damage. However, decrease of tortuosity factor was found after redox treatment. Tortuosity factor is largely related with connectivity and particle size. YSZ connectivity change was little after redox treatment as shown in Fig. 13 (a), but mean interception length of YSZ increased after redox treatment as shown in Fig. 13(c). From Fig. 12(b), we can find that YSZ particle distribution show smaller change than the Ni phase. But YSZ particle distribution seems to be slightly shifted to larger interception length after 4 redox cycle test. This change is consistent with the change of YSZ tortuosity factor shown in Fig. 10(b). Increase of mean interception length of YSZ is also consistent with the decrease of YSZ specific surface area as shown in Fig. 13(b). However, precise phenomenon is not clear. YSZ tortuosity factor decreased for "4 redox and 20 h discharge" sample, but increased after "10 redox and 20 h discharge" as shown in Fig. 10(d). In addition, we can see that YSZ connectivity decreases as redox cycles are repeated as shown in Table 2. Destruction of YSZ network might have taken place as redox cycles are repeated.

Gradual increase of polarization resistance does not correspond to the increase of active TPB density during redox cycles. Furthermore, gradual increase of ohmic resistance is not clearly explained from the present microstructure analysis. As we have shown in

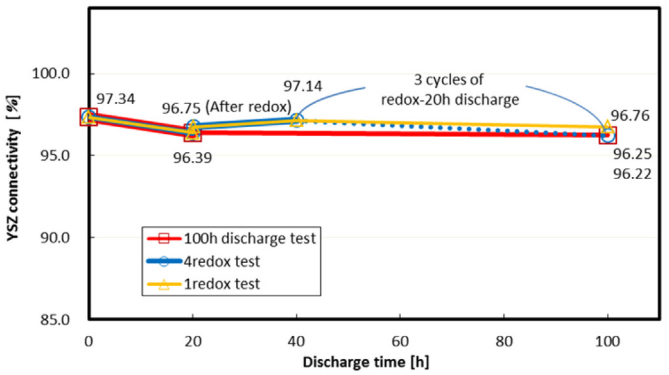

(a)

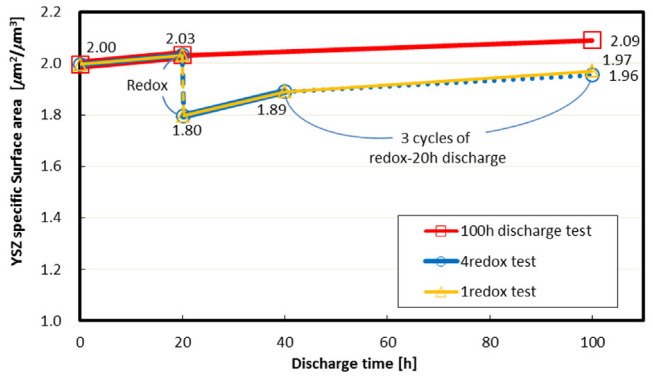

(b)

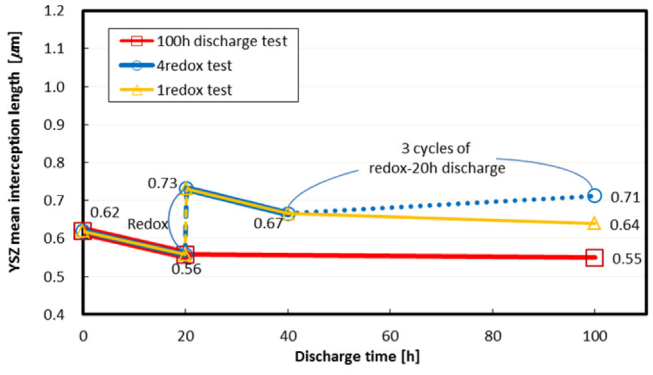

(c)

Fig. 13. Change of (a) YSZ connectivity, (b) YSZ specific surface area, and (c) YSZ mean interception length.

Fig. 2(a), ohmic resistance show an increase during discharge process without redox treatment. The reason of this increase is not clear, but might be attributed to the degradation of the electrolyte. If anode is delaminated from the electrolyte, it is considered that the ohmic resistance should increase discontinuously after the responsible redox treatment. Thus, electrode delamination does not seem to be the critical reason for the increase of ohmic resistance in the present study. Other degradation mechanisms should be considered. There are several reports on microstructure change using TEM. Chen et al. [27] reported a formation of NiO ribbon phase along Ni-YSZ interface under hydrogen atmosphere. Also, formation of tetragonal YSZ and the associated decrease of ionic conductivity are reported by several groups [28–31]. These cannot be analyzed through the microstructure analysis of FIB-SEM. There is a possibility that such nano-scale phenomena might have caused gradual degradation of the anode performance during redox cycles.

5. Conclusion

Relationship between cell performance and microstructure change of anode during redox cycles was analyzed. From the anode voltage measurements, cell performance enhanced just after the redox treatment and decreased during the subsequent discharge operation. Polarization resistance decreased just after the redox treatment and increased during the discharge process. As redox cycles are repeated, polarization resistance gradually increased. Ohmic resistance kept increasing during the whole discharge process.

From the microstructure analysis, active TPB density increases after the redox treatment and decreases after the discharge process, which is accompanied by the changes of Ni connectivity and Ni specific surface area. These results are consistent with the decrease of polarization resistance after each redox treatment and the increase during each subsequent discharge process.

From comparison of reconstructed microstructures with different number of redox cycles, TPB density increased as redox cycles are repeated. This is inconsistent with the electrochemical measurement which shows gradual increase of polarization resistance. Therefore, cell performance change during redox cycles cannot be explained only from the microstructure change. Another factor such as phase transition of YSZ or change of local chemical reaction kinetics should be further investigated.

Acknowledgments

This work was partly supported by New Energy and Industrial Technology Development Organization (NEDO).

References

[1] T. Klemenso, M. Mogensen, J. Am. Ceram. Soc. 90 (11) (2007) 3582–3588.
[2] M. Ettler, H. Timmermann, J. Malzbender, A. Weber, N.H. Menzler, J. Power Sources 195 (2010) 5452.
[3] D. Sarantaridis, A. Atkinson, Fuel Cells 07 (3) (2007) 246–258.
[4] M. Pihlatie, A. Kaiser, M. Mogensen, Solid State Ionics 180 (2009) 1100–1112.
[5] A. Faes, A. Nakajo, A. Hessler-Wyser, D. Dubois, A. Brisse, S. Modena, J.V. Herle, J. Power Sources 193 (2009) 55–64.
[6] A. Faes, Z. Wuillemin, P. Tanasini, N. Accardo, J.V. Herle, J. Power Sources 196 (2011) 3553–3558.
[7] Q. Ma, F. Tietz, A. Leonide, E. Ivers-Tiffée, Electrochem. Commun. 12 (2010) 1326–1328.
[8] J. Laurencin, G. Delette, O. Sicardy, S. Rosini, F. Lefebvre-Joud, J. Power Sources 195 (2010) 2747–2753.
[9] D. Fouquet, A.C. Muller, A. Weber, E. Ivers-Tiffee, Ionics 8 (2003) 103–108.
[10] H. Sumi, R. Kishida, J.Y. Kim, H. Muroyama, T. Matsui, K. Eguchi, J. Electrochem. Soc. 157 (12) (2010) B1747–B1752.
[11] Q. Jeangros, A. Faes, J.B. Wagner, T.W. Hansen, U. Aschauer, J. Van herle, A. Hessler-Wyser, R.E. Dunin-Borkowski, Acta Mater. 58 (2010) 4578–4589.
[12] N.M. Tikekar, T.J. Armstrong, A.V. Virkar, J. Electrochem. Soc. 153 (4) (2006) A654–A663.
[13] J. Laurencin, V. Roche, C. Jaboutian, I. Kieffer, J. Mougin, M.C. Steil, Int. J. Hydrogen. Energy 37 (2012) 12557–12573.
[14] J.L. Young, V.I. Briss, J. Power Sources 196 (2011) 7126–7135.
[15] M.H. Pihlatie, A. Kaiser, M.B. Mogensen, Solid State Ionics 222-223 (2012) 38–46.
[16] M.H. Pihlatie, A. Kaiser, M. Mogensen, M. Chen, Solid State Ionics 180 (2011) 82–90.
[17] H. Iwai, N. Shikazono, T. Matsui, H. Teshima, M. Kishimoto, R. Kishida, D. Hayashi, K. Matsuzaki, D. Kanno, M. Sato, H. Muroyama, K. Eguchi, N. Kasagi, H. Yoshida, J. Power Sources 195 (2010) 955–961.
[18] D. Kanno, N. Shikazono, N. Takagi, K. Matsuzaki, N. Kasagi, J. Electrochem. Acta 56 (2012) 4015–4021.
[19] K. Matsuzaki, N. Shikazono, N. Kasagi, J. Power Sources 196 (2011) 3073–3082.
[20] N. Shikazono, D. Kanno, K. Matsuzaki, H. Teshima, S. Sumino, N. Kasagi, J. Electrochem. Soc. 157 (5) (2010) B665–B672.
[21] K. Eguchi1, N. Kamiuchi, J.-Y. Kim, H. Muroyama, T. Matsui, M. Kishimoto, M. Saito, H. Iwai, H. Yoshida, N. Shikazono, N. Kasagi, J. Akikusa, H. Eto, D. Ueno, M. Kawano, T. Inagaki, Fuel Cells 12 (4) (2012) 537–542.
[22] D. Waldbillig, A. Wood, D.G. Ivey, J. Power Sources 145 (2005) 206–215.

[23] M. Pihlatie, T. Ramos, A. Kaiser, J. Power Sources 193 (2009) 322–330.
[24] Z. Jiao, N. Shikazono, N. Kasagi, J. Electrochem. Soc. 159 (3) (2012) B285–B291.
[25] L. Holzer, B. Iwanschitz, Th Hocker, B. Münch, M. Prestat, D. Wiedenmann, U. Vogt, P. Holtappels, J. Sfeir, A. Mai, Th Graule, J. Power Sources 196 (2011) 1279–1294.
[26] L. Holzer, B. Iwanschitz, Th Hocker, L. Keller, O. Pecho, G. Sartoris, Ph Gasser, B. Muench, J. Power Sources 242 (2013) 179–194.
[27] Yun Chen, Song Chen, Gregory Hackett, Harry Finklea, Xueyan Song, Kirk Gerdes, Solid State Ionics 87 (2011) 204–205.
[28] Song Chen, Yun Chen, Harry Finklea, Xueyan Song, Gregory Hackett, Kirk Gerdes, Solid State Ionics 206 (2012) 104–111.
[29] Taro Shimonosono, Haruo Kishimoto, Manuel E. Brito, Katsuhiko Yamaji, Teruhisa Horita, Harumi Yokokawa, Solid State Ionics 225 (2012) 69–72.
[30] M. Hattori, Y. Takeda, J.-H. Lee, S. Ohara, K. Mukai, T. Fukui, S. Takahashi, Y. Sakaki, A. Nakanishi, J. Power Sources 131 (2004) 247–250.
[31] W.G. Coors, J.R. O'Brien, J.T. White, Solid State Ionics 180 (2009) 246–251.